



Pettini, M., Zych, B. J., Muprhy, M. T. et al.(2008). Deuterium abundance in the most metal-poor damped Lyman alpha system: converging on $\Omega(b,0)h(2)$.

Originally published in *Monthly Notices of the Royal Astronomical Society*, 391(4), 1499-1510

Available from:

<http://dx.doi.org/10.1111/j.1365-2966.2008.13921.x>

This version of the article copyright © 2008 The Authors.

This is the author's version of the work. It is posted here with the permission of the publisher for your personal use. No further distribution is permitted. If your library has a subscription to this journal, you may also be able to access the published version via the library catalogue.

The definitive version is available at www.interscience.wiley.com.



Deuterium Abundance in the Most Metal-Poor Damped Lyman alpha System: Converging on $\Omega_{b,0}h^2$

Max Pettini¹, Berkeley J. Zych¹, Michael T. Murphy^{2,1}, Antony Lewis¹ and Charles C. Steidel³

¹*Institute of Astronomy, University of Cambridge, Madingley Road, Cambridge CB3 0HA, UK*

²*Centre for Astrophysics and Supercomputing, Swinburne University of Technology, Mail H39, PO Box 218, Victoria 3122, Australia*

³*California Institute of Technology, Mail Stop 105-24, Pasadena, CA 91125, USA*

Accepted —; Received —; in original form —

ABSTRACT

The most metal-poor DLA known to date, at $z_{\text{abs}} = 2.61843$ in the spectrum of the QSO Q0913+072, with an oxygen abundance only $\sim 1/250$ of the solar value, shows six well resolved DI Lyman series transitions in high quality echelle spectra recently obtained with the ESO VLT. We deduce a value of the deuterium abundance $\log(D/H) = -4.56 \pm 0.04$ which is in good agreement with four out of the six most reliable previous determinations of this ratio in QSO absorbers. We find plausible reasons why in the other two cases the 1σ errors may have been underestimated by about a factor of two. The addition of this latest data point does not change significantly the mean value of the primordial abundance of deuterium, suggesting that we are now converging to a reliable measure of this quantity. We conclude that $\langle \log(D/H)_p \rangle = -4.55 \pm 0.03$ and $\Omega_{b,0}h^2(\text{BBN}) = 0.0213 \pm 0.0010$ (68% confidence limits). Including the latter as a prior in the analysis of the five year data of *WMAP* leads to a revised best-fitting value of the power-law index of primordial fluctuations $n_s = 0.956 \pm 0.013$ (1σ) and $n_s < 0.990$ with 99% confidence. Considering together the constraints provided by *WMAP* 5, $(D/H)_p$, baryon oscillations in the galaxy distribution, and distances to Type Ia supernovae, we arrive at the current best estimates $\Omega_{b,0}h^2 = 0.0224 \pm 0.0005$ and $n_s = 0.959 \pm 0.013$.

Key words:

1 INTRODUCTION

The exquisite precision with which the temperature anisotropies of the cosmic microwave background (CMB) have been mapped on the sky has allowed the determination of cosmological parameters to better than 10% (Dunkley et al. 2008). It is still important, however, to measure these parameters with alternative methods, partly as a consistency check on the standard cosmological model, but also because the CMB fluctuations generally constrain *combinations* of more than one parameter (e.g. Bridle et al. 2003). The contribution of baryons to the present-day critical density, $\Omega_{b,0}h^2$ where as usual $h = H_0/100 \text{ km s}^{-1} \text{ Mpc}^{-1}$, is one such example: the value of $\Omega_{b,0}h^2$ which best fits the power spectrum of CMB fluctuations is tied to other parameters, such as the spectral index of primordial density perturbations, n_s , and the optical depth to reionisation, τ (see, for example, Pettini 2006).

The quantity $\Omega_{b,0}h^2$ can also be deduced from the primordial abundances of the light elements whose nucleosyn-

thesis is the result of physical processes that are entirely different from the acoustic oscillations of the photon-baryon fluid imprinted on the CMB, and that took place at much earlier times—only a few hundred seconds, rather than a few hundred thousand years, after the Big Bang. Among the light elements produced by primordial nucleosynthesis, deuterium is the one whose abundance by number relative to hydrogen, $(D/H)_p$, depends most sensitively on $\Omega_{b,0}h^2$, and is thus the ‘baryometer’ of choice (Steigman 2007; Molaro 2008).

Reliable measures of $(D/H)_p$ are difficult to obtain, however. The astrophysical environments which seem most appropriate are the hydrogen-rich clouds absorbing the light of background QSOs at high redshifts, but rare combinations of: (a) neutral hydrogen column density in the range $17 \lesssim \log[N(\text{H I})/\text{cm}^{-2}] \lesssim 21$; (b) low metallicity $[M/H]$ corresponding to negligible astration of D; and (c) most importantly, low internal velocity dispersion of the absorbing atoms allowing the isotope shift of only 81.6 km s^{-1} to be

adequately resolved, are required for this observational test to succeed. Thus, while the potential of this method was appreciated more than thirty years ago (Adams 1976) and first realised with the advent of 8-10 m class telescopes in the 1990s (Tytler et al. 1995), the number of trustworthy measurements of $(D/H)_p$ is still only five or six (O’Meara et al. 2006; Steigman 2007).

There are a strong incentives to increase these measure statistics. On the one hand, the mean $\langle (D/H)_p \rangle = (2.82 \pm 0.26) \times 10^{-5}$ implies $\Omega_{b,0} h^2 (\text{BBN}) = 0.0213 \pm 0.0013$ (O’Meara et al. 2006) which agrees, within the errors, with the value $\Omega_{b,0} h^2 (\text{CMB}) = 0.02273 \pm 0.00062$ obtained by Dunkley et al. (2008) from the analysis of five years of observations with the *Wilkinson Microwave Anisotropy Probe (WMAP 5)*. On the other hand, the standard deviation among the six measures of $(D/H)_p$ in high redshift QSO absorbers exceeds the dispersion expected from the individual errors (leading to a high value of χ^2 of the six measurements about the weighted mean). This is probably due to the considerable difficulties in accounting for the full measurement errors (random and systematic) of astronomical observations, but is nevertheless a source of concern, particularly when viewed in conjunction with the as yet poorly understood dispersion of D/H values in the Milky Way (Linsky et al. 2006).

Additional measurements of the D/H ratio at high redshift should, in principle at least, lead to a more precise estimate of $(D/H)_p$, as well as to a better assessment of the reasons for the scatter of the existing values. Such improvements are not only of interest in a cosmological context, but are also relevant to Galactic chemical evolution models in which the degree of astration of D is an important diagnostic (e.g. Romano et al. 2006; Steigman, Romano & Tosi 2007). In this paper, we report observations of deuterium absorption in a seventh high redshift absorber, a very metal-poor damped Ly α system (DLA) at $z_{\text{abs}} = 2.61843$, and consider their implications for the determination of $(D/H)_p$, $\Omega_{b,0} h^2$, and other cosmological parameters.¹

2 OBSERVATIONS

The existence of a metal-poor DLA at $z_{\text{abs}} = 2.61843$ in the line of sight to the bright ($V = 17.1$), $z_{\text{em}} = 2.785$, QSO Q0913+072 has been known for some time (Pettini et al. 1997; Ledoux et al. 1998; Erni et al. 2006). More recently, it has been realised that DLAs of low metallicity are also likely to have simple kinematics, possibly reflecting an underlying mass-metallicity relation of the host dark-matter halos (Ledoux et al. 2006; Murphy et al. 2007; Prochaska et al. 2008; Pontzen et al. 2008). The most metal-poor DLAs are thus likely to be among the most promising candidates for follow-up high-resolution spectroscopy aimed at resolving the isotope shift in high order lines of the Lyman series.

To this end, we targeted Q0913+072 with a concerted series of observations in 2007, using UVES (Dekker et al. 2000) on the ESO VLT2. The data were acquired in service

mode; including a few spectra retrieved from the UVES data archive, the total exposure time devoted to this QSO was 77 550 s. Details of the data reduction process can be found in Pettini et al. (2008); briefly, the final reduced and combined spectrum covers the wavelength region from 3310 Å to 9280 Å with a resolution of 6.7 km s^{-1} FWHM, sampled with ~ 3 pixels. The signal-to-noise ratio in the continuum varies from $S/N \simeq 35$ per pixel at the redshifted wavelength of the damped Ly α line, to $S/N \simeq 15$ just longwards of the Lyman limit of the $z_{\text{abs}} = 2.61843$ DLA.

Pettini et al. (2008) presented an analysis of the chemical composition and kinematics of this and other metal-poor DLAs, from consideration of metal absorption lines due to H, C, N, O, Al, Si, and Fe; we refer the interested reader to that paper for details. Of relevance to the present work are the following main results. With relative abundances $[C/H] = -2.75$ and $[Fe/H] = -2.80$ the $z_{\text{abs}} = 2.61843$ system in Q0913+072 is the most metal-poor DLA known.² Its oxygen abundance, $[O/H] = -2.37$, is also among the lowest recorded in damped systems. The metal lines arising in the neutral gas have a very simple kinematic structure, consisting of two components at $z_{\text{abs}} = 2.61828$ and $z_{\text{abs}} = 2.61843$ ($\Delta v = 12.4 \text{ km s}^{-1}$), with low internal velocity dispersions, $b = 3.7 \text{ km s}^{-1}$ and 5.4 km s^{-1} respectively (where $b = \sqrt{2}\sigma$ and σ is the one dimensional velocity dispersion of the absorbing atoms along the line of sight). The column density of neutral gas is distributed between the two components in approximately 3:7 proportion (see Figure 1 and Table 2 of Pettini et al. 2008).

While these characteristics bode well for the possibility of resolving the D component of the Lyman series lines, they do not guarantee it. It is often the case that partially ionised gas at nearby velocities, with optical depths too low to be recognised in the metal lines, can blend with the H and D absorption due to the DLA itself, and prevent a reliable measurement of $N(\text{D I})$. Partially ionised gas does in fact appear to contribute to the C II absorption lines in this DLA, but seems to be confined to positive, rather than negative, velocities relative to $z_{\text{abs}} = 2.61843$. As can be seen from Fig. 1, this is indeed, somewhat fortuitously, the case.

3 HYDROGEN AND DEUTERIUM ABSORPTION IN THE $Z_{\text{ABS}} = 2.61843$ DLA

3.1 Deuterium

In Fig. 1 we have reproduced on a velocity scale relative to $z_{\text{abs}} = 2.61843$ the normalised profiles of absorption lines in the Lyman series of the DLA, from Ly α to Ly10. Ly11 is also visible in the Ly10 panel, while higher order lines are all blended with one another, constituting an ‘effective’ Lyman limit from $\lambda_0 = 917 \text{ Å}$. It is clear from the high order transitions that there is H I absorption at positive velocities relative the $z_{\text{abs}} = 2.61843$ DLA, extending to $v \simeq +200 \text{ km s}^{-1}$. On the blue side, however, there appears to be no additional components over those seen in the metal lines, and the D I absorption is clearly resolved in Ly δ , and Ly7 through to Ly11, six transitions in total. (In Ly α , Ly β and Ly γ , which

¹ Damped Ly α systems are a class of QSO absorbers defined by their high column densities of neutral hydrogen, $\log[N(\text{H I})/\text{cm}^{-2}] \geq 20.3$; see Wolfe, Gawiser, & Prochaska (2005), and Pontzen et al. (2008) for recent reviews of DLAs.

² With the usual definition, $[X/H] \equiv \log(X/H)_{\text{DLA}} - \log(X/H)_{\odot}$.

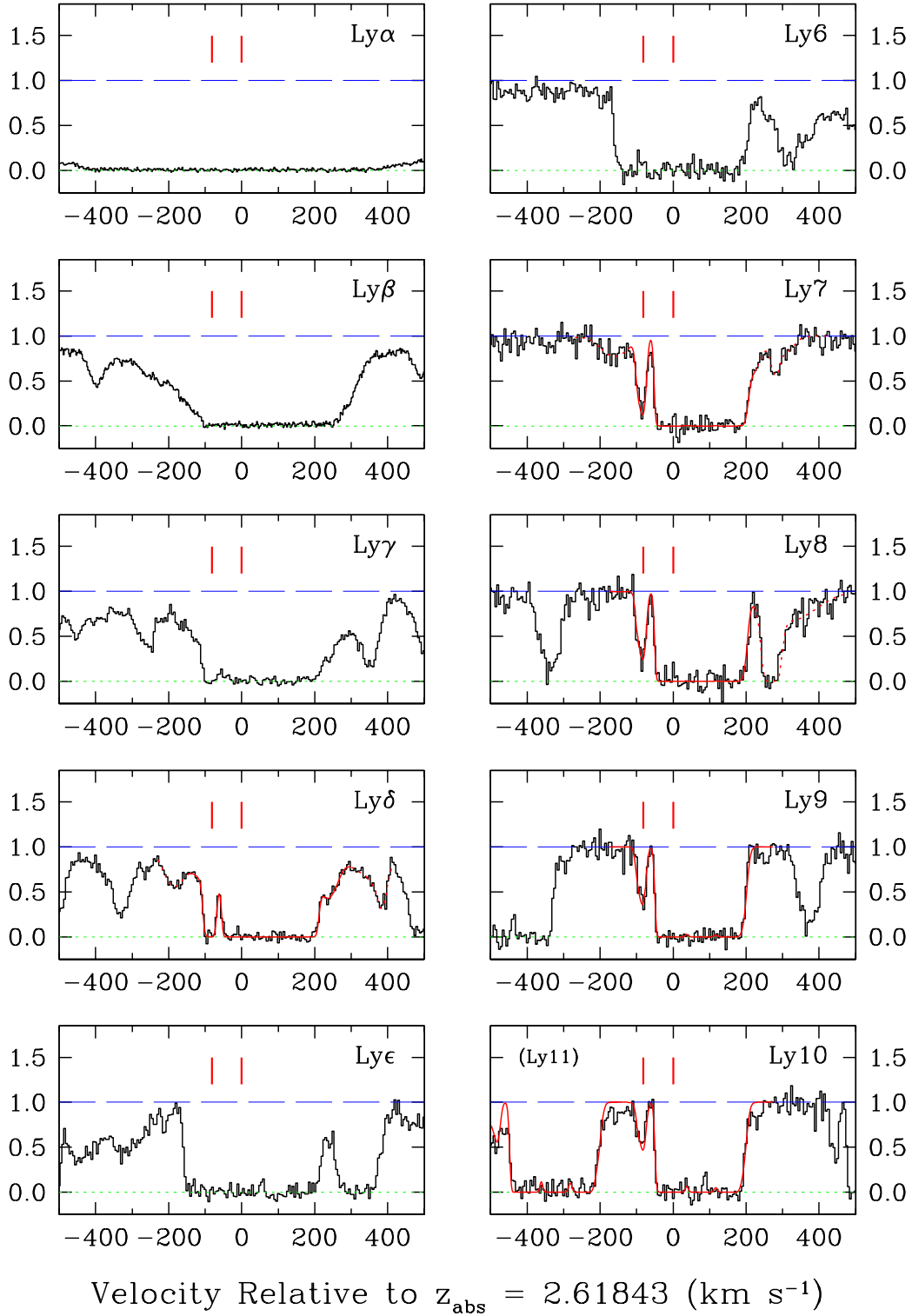


Figure 1. Observed profiles (black histograms) and fitted Voigt profiles (continuous red lines) of absorption lines in the Lyman series of the $z_{\text{abs}} = 2.61843$ DLA in Q0913+072. The y -axes of the plots show relative intensity. The two vertical tick marks in each panel indicate the expected locations of the main absorption component of the DLA in, respectively, H I (at $v = 0 \text{ km s}^{-1}$ in the plots) and D I (at $v = -81.6 \text{ km s}^{-1}$). A second absorption component, centred at $v = -12.4 \text{ km s}^{-1}$, is resolved in the metal lines associated with this DLA, but the two components are blended in the intrinsically broader H I and D I absorption. Additional H I absorption is seen at positive velocities relative to the DLA, but its column density is ~ 100 times lower than that of the DLA, and therefore does not contribute to the observed D I absorption lines (see text).

Table 1. Absorption components fitted to the $z_{\text{abs}} = 2.61843$ DLA in Q0913+072.

Ion	z_{abs}	b (km s ⁻¹)	Fraction
H I ^a	2.61828 ^b	11.9 ^c	0.33 ^d
H I ^a	2.61843 ^b	11.1 ^c	0.67 ^d
D I	2.61828 ^b	8.6	0.33
D I	2.61843 ^b	8.7	0.67
O I	2.61828	3.5	0.31
O I	2.61843	5.2	0.69

^aAdditional components at positive velocities relative to $z_{\text{abs}} = 2.61843$ were fitted to the H I lines.

^bFixed to be the same as O I.

^cPoorly determined because all H I lines are saturated and blended.

^dFixed to be the same as D I.

have the highest transition probabilities, H I and D I are intrinsically blended, whereas in Ly ϵ and Ly6 presumably unrelated absorption in the Lyman forest is blended with the absorption due to the DLA).

The availability of many D I transitions with a range of optical depths, from the saturated Ly δ to the optically thin Ly10 and Ly11, allows for a precise determination of the column density $N(\text{D I})$. To this end, we fitted the profiles of the Lyman lines where the D I absorption is resolved with theoretical Voigt profiles generated by the VPFIT (version 8.02) software package.³ VPFIT uses χ^2 minimisation to deduce the values of redshift z , logarithmic column density $\log[N/(\text{cm}^{-2})]$, and Doppler parameter b (km s⁻¹) that best reproduce the observed absorption line profiles, taking into account the instrumental broadening function in its χ^2 minimisation and error evaluation. We used the compilation of laboratory wavelengths λ_{lab} and f -values by Morton (2003). In Table 1 we have collected relevant details of the absorption model fitted to the observed line profiles in Fig. 1; the corresponding theoretical profiles generated by VPFIT are shown with continuous red lines in Fig. 1.

As mentioned in Section 2, the metal lines detected in this DLA consist of two components (Pettini et al. 2008), with the parameters listed in Table 1 for O I. The two components are not clearly distinguished in D I because: (i) absorption by the lighter D is intrinsically broader (see discussion below), and (ii) the S/N ratio of the spectrum is lower at the shorter wavelengths of the high order Lyman lines (at $z_{\text{abs}} = 2.61843$ the wavelength region between Ly δ and the Lyman limit is redshifted to $\lambda_{\text{obs}} = 3438\text{--}3318$ Å, approaching the cut-off by atmospheric ozone). Thus, in the first step of the fitting process, we fixed the redshifts of the two components to be the same as those determined from the metal lines while keeping the values of b and $N(\text{D I})$ as free parameters to be optimised by VPFIT. The best fitting values of b and $N(\text{D I})$ thus reached are consistent with those deduced for O I and other metal lines. The relative proportions of atoms between the two components are similar in all species and the b -values are broader in D than in O, as expected. Recall that the velocity dispersion of an absorption line is the

quadratic combination of macroscopic (turbulence) and microscopic (temperature related) terms, i.e. $b_{\text{tot}}^2 = b_{\text{turb}}^2 + b_{\text{T}}^2$; while the former is presumably the same for all elements, the latter has an inverse dependence on the square root of the mass, since $b_{\text{T}}^2 = 2kT/m$ (e.g. Strömberg 1948). The higher b -values of the two absorption components in D than O imply temperatures of a few thousand degrees.

The model parameters listed in Table 1 correspond to a best fitting value for the column density of D I (sum of the two components) of

$$\log[N(\text{D I})/\text{cm}^{-2}] = 15.78 \pm 0.02,$$

but we stress that this value does *not* depend on the details of the ‘cloud’ model adopted. To test its robustness, we rerun VPFIT without any assumptions about the distribution of velocities of the absorbers. Using as a starting point a single absorbing component with unspecified redshift and b -value, VPFIT returned a best-fitting value, $\log[N(\text{D I})/\text{cm}^{-2}] = 15.79 \pm 0.02$, that is only 0.01 dex higher than that obtained with the parameters in Table 1 (although this second model results in a higher value of χ^2 between computed and observed profiles). Any other adjustment to the details of the profile fits, such as varying the relative proportions of D I between the two components and their b -values, or changing the parameters of nearby absorption in the Lyman forest, resulted in even smaller differences in the total value of $\log N(\text{D I})$ returned by VPFIT.

As a final comment here, we point out that the VPFIT-generated line profiles shown in Figure 1 include a number of other components to the red of $z_{\text{abs}} = 2.61843$, required to reproduce the saturated profiles of the H I Lyman lines which extend to $v \simeq 200$ km s⁻¹. The parameters of these extra absorptions are poorly constrained, but do not influence the determination of $\log N(\text{D I})$ because they involve column densities of less than $\sim 1/100$ that of the DLA and thus do not contribute to the observed D I absorption.

3.1.1 Consistency check with the apparent optical depth method

Since the D I absorption lines we observe are resolved, we can deduce the column density directly from the measured residual intensity in each wavelength, or velocity, interval across the absorption lines (e.g. Hobbs 1974). The apparent optical depth at velocity v , $\tau_a(v)$, is related to the observed intensity in the line, $I_{\text{obs}}(v)$, by

$$\tau_a(v) = -\ln [I_{\text{obs}}(v)/I_0(v)], \quad (1)$$

where $I_0(v)$ is the intensity in the continuum. With the assumption of negligible smearing of the intrinsic line profile by the instrumental broadening function, we have:

$$\tau(v) \approx \tau_a(v). \quad (2)$$

The optical depth $\tau(v)$ is in turn related to the column density of D I atoms in each velocity bin, $N(v)$ in units of $\text{cm}^{-2} (\text{km s}^{-1})^{-1}$, by the expression

$$N(v) = \frac{\tau(v)}{f\lambda} \times \frac{m_e c}{\pi e^2} = \frac{\tau(v)}{f\lambda(\text{Å})} \times 3.768 \times 10^{14} \quad (3)$$

where the symbols f , λ , c , e and m_e have their usual meanings.

³ VPFIT is available from <http://www.ast.cam.ac.uk/~rfc/vpfit.html>

Table 2. Results of apparent optical depth analysis of D I lines

Transition	λ_{lab}^a (Å)	f^a	$N_{\text{TOT}}(\text{D I})$ (10^{15} cm^{-2})
D I Ly7	925.9737	0.003184	$5.64^{+0.43}_{-0.25}$
D I Ly8	922.899	0.002216	$6.35^{+0.40}_{-0.29}$
D I Ly9	920.712	0.001605	$6.08^{+0.37}_{-0.32}$
D I Ly10	919.102	0.001201	$5.61^{+0.41}_{-0.37}$
Weighted Mean			$5.93^{+0.21}_{-0.16}$

^aMorton (2003).

As emphasized by Savage & Sembach (1991), the attraction of the apparent optical depth method lies in the fact that no assumption has to be made concerning the velocity distribution of the absorbers. Furthermore, this method provides a consistency check when two or more transitions arising from the same atomic energy level, but with different values of the product $f\lambda$, are analyzed, as is the case here. The run of $N(v)$ with v should be the same, within the errors in $I_{\text{obs}}(v)$, for all such lines.

For D I in Q0913+072, we can apply to apparent optical depth analysis to four unsaturated transitions, from Ly 7 to Ly 10; the other lines in the D I Lyman series being either partly blended or saturated (see Figure 1). For each transition, we deduced a value of $N(\text{D I})$ by summing eq. (3) over the n velocity bins which make up the absorption profile:

$$N_{\text{TOT}} = \sum_{i=1}^n N_i(v). \quad (4)$$

From the known error in the value of $I_{\text{obs}}(v)$ in each velocity bin, $\delta I_{\text{obs}}(v)$, we calculated the error δN_{TOT} :

$$\delta N_{\text{TOT}}^2 = \sum_{i=1}^n \delta N_i(v)^2, \quad (5)$$

which is asymmetric about N_{TOT} because of the non-linear nature of eq. (1).

Figure 2 shows the run of $N_i(v)$ across the four D I absorption lines, while values of N_{TOT} and δN_{TOT} are listed in Table 2. As can be seen from Figure 2 and Table 2, the four D I absorption lines are in good mutual agreement, and the standard deviation between the four independent measures of $N(\text{D I})$ is $1\sigma = 0.35 \times 10^{15} \text{ cm}^{-2}$, or $\sim 6\%$ of the mean. The weighted mean of the four values of $N(\text{D I})$ returned by the apparent optical depth analysis is $\langle N(\text{D I}) \rangle = (5.93^{+0.21}_{-0.16}) \times 10^{15} \text{ cm}^{-2}$, where the uncertainties quoted are the errors on the weighted mean. On a logarithmic scale $\log[N(\text{D I})/\text{cm}^{-2}] = 15.775 \pm 0.014$, in very good agreement (as expected) with the value of $\log[N(\text{D I})/\text{cm}^{-2}] = 15.78 \pm 0.02$ returned by VPFIT, which we retain in the subsequent analysis.

3.2 Hydrogen

Fig. 3 shows the region encompassing the damped Ly α line. In principle, the column density of neutral hydrogen should be tightly constrained from the shape of the damping wings

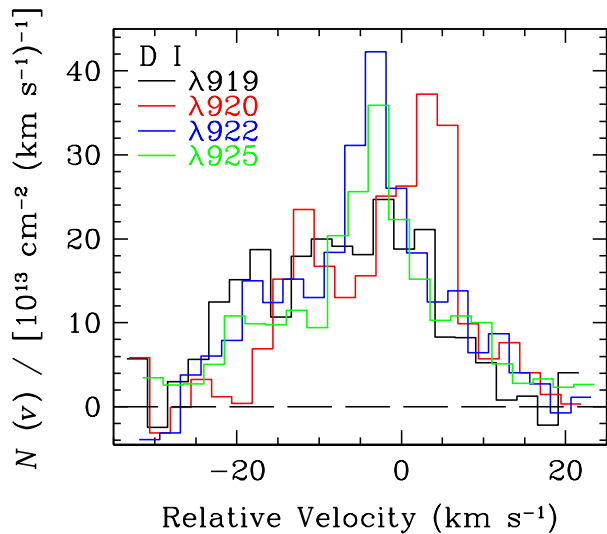


Figure 2. Apparent optical depth analysis: column density as a function of velocity for the four unsaturated and unblended D I lines in the $z_{\text{abs}} = 2.61843$ DLA in Q0913+072. The transitions shown in the legend are in increasing order of $f\lambda$ from the top. Values of $N_{\text{TOT}}(\text{D I})$ are collected in Table 2.

which extend over many hundreds of pixels (and are thus extremely well sampled by the data). In practice, the limiting factors are the uncertainty in the determination of the continuum level (to which the absorption is normalised) and the overlapping absorption from the narrower lines in the Ly α forest. After numerous trials varying the continuum level and the weights given to different spectral intervals deemed to be free of overlapping absorption (see Kirkman et al. 2003 for a more extensive discussion of the problem) we converged on the best fitting value:

$$\log[N(\text{H I})/\text{cm}^{-2}] = 20.34 \pm 0.04;$$

the corresponding theoretical damped profile is overplotted on the data in Fig. 3.

It is difficult to estimate reliably the systematic error which may be affecting this determination. While consistent with the above estimate of $\log N(\text{H I})$ from Ly α , the higher order Lyman lines do not help to reduce the error further because they are all saturated and their equivalent widths include uncertain contributions from the lower column density components to the red of the DLA. In future, it may be possible to improve on the accuracy with which values $N(\text{H I})$ can be deduced from the analysis of damped profiles buried within the Ly α forest by developing more sophisticated statistical methods to deal with the overlapping absorption, perhaps analogous to those used to subtract foreground Galactic emission from maps of the CMB. For the moment, we can perhaps obtain an indication of the magnitude of the systematic uncertainty in $N(\text{H I})$ by considering three previous estimates of this quantity, reported by different authors who used different spectrographs and telescopes, as follows: $\log[N(\text{H I})/\text{cm}^{-2}] = 20.36 \pm 0.08$ (Pettini et al. 1997); 20.2 ± 0.1 (Ledoux et al. 1998); 20.36 ± 0.05 (Erni et al. 2006). Of these, only the last one refers to a (small) subset of the data used here. From these results it appears

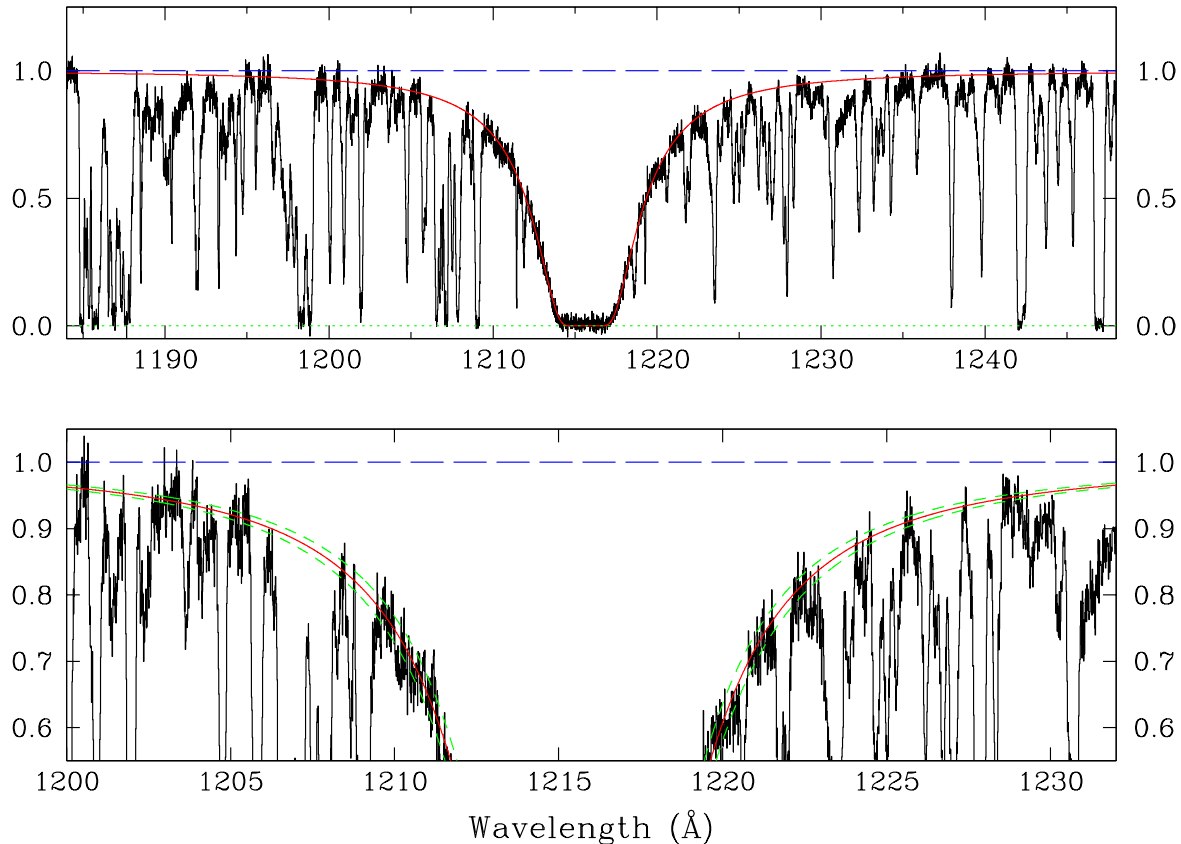


Figure 3. *Top:* Portion of the normalised spectrum of Q0913+072 encompassing the damped Ly α line at $z_{\text{abs}} = 2.61843$ (black histogram). The continuous red line shows the theoretical profile for a neutral hydrogen column density $\log[N(\text{H I})/\text{cm}^{-2}] = 20.34$. *Bottom:* Expanded portion of the upper plot on a scale chosen to illustrate the sensitivity of the damping wings to the column density of neutral hydrogen. The short-dash green lines correspond to the ± 0.04 limits to the best fitting value $\log[N(\text{H I})/\text{cm}^{-2}] = 20.34$. In both panels the y -axis is residual intensity.

that our present estimate, $\log[N(\text{H I})/\text{cm}^{-2}] = 20.34 \pm 0.04$, is unlikely to be in error by more than the stated margin.

From the values of $N(\text{D I})$ and $N(\text{H I})$ deduced in sections 3.1 and 3.2, we arrive at the determination of the deuterium abundance in the $z_{\text{abs}} = 2.61843$ DLA in line to Q0913+072 of:

$$\log(\text{D}/\text{H}) = -4.56 \pm 0.04$$

(where the errors have been combined in quadrature).

4 THE PRIMORDIAL ABUNDANCE OF DEUTERIUM

In Table 3 we have collected relevant measurements for all the high redshift QSO absorption systems where the isotope shift has been resolved in absorption lines of the Lyman series. This prime sample of what are generally considered to be the most reliable measures of D/H at high z now consists of seven independent determinations. Other reports in the literature (e.g. Levshakov et al. 2002; Chrichton et al. 2004), while still interesting, refer to spectra of less straightforward interpretation because not all the D I components are resolved, so that the values of D/H deduced are more

dependent on the precise description of the kinematics of the gas than is the case for the seven absorbers listed in Table 3 (see also the discussions of this point by Kirkman et al. 2003 and O’Meara et al. 2006).

All the measurements of D/H in Table 3 should be representative of the primordial abundance $(\text{D}/\text{H})_{\text{p}}$, because in all seven cases the gas has undergone little chemical enrichment, as evidenced by the low abundance of O (and other heavy elements), less than 1/10 of solar (see column 5 of Table 3). For comparison, the total degree of astration of D over the lifetime of the Milky Way amounts to only $\lesssim 20\%$, if one accepts the possibility that in the local interstellar medium some of the deuterium may be depleted onto dust grains (Linsky et al. 2006). Theoretically, galactic chemical evolution models (e.g. Prantzos & Ishimaru 2001; Romano et al. 2006) show negligible reduction in D/H from the primordial value when the gas metallicities are as low as those of the seven QSO absorbers in Table 3, while observationally no trend is observed between D/H and O/H (Pettini 2006). Dust depletion of D is not expected to be an issue here, given the very low depletions of even the most refractory elements at these low levels of chemical enrichment (e.g. Akerman et al. 2005).

We arrive at an estimate of $\log(\text{D}/\text{H})_{\text{p}}$ by averaging

Table 3. PRIME SAMPLE OF D/H MEASUREMENTS IN QSO ABSORPTION LINE SYSTEMS

QSO	z_{em}	z_{abs}	$\log N(\text{H I})$ (cm^{-2})	[O/H] ^b	$\log(\text{D/H})$	Ref. ^a
HS 0105+1619	2.640	2.53600	19.42 ± 0.01	-1.70	-4.60 ± 0.04	1
Q0913+072	2.785	2.61843	20.34 ± 0.04	-2.37	-4.56 ± 0.04	2, 3
Q1009+299	2.640	2.50357	17.39 ± 0.06	$< -0.67^{\text{c}}$	-4.40 ± 0.07	4
Q1243+307	2.558	2.52566	19.73 ± 0.04	-2.76	-4.62 ± 0.05	5
SDSS J155810.16-003120.0	2.823	2.70262	20.67 ± 0.05	-1.47	-4.48 ± 0.06	6
Q1937-101	3.787	3.57220	17.86 ± 0.02	< -0.9	-4.48 ± 0.04	7
Q2206-199	2.559	2.07624	20.43 ± 0.04	-2.04	-4.78 ± 0.09	2, 8

^aReferences—1: O’Meara et al. (2001); 2: Pettini et al. (2008); 3: This work; 4: Burles & Tytler (1998b); 5: Kirkman et al. (2003); 6: O’Meara et al. (2006); 7: Burles & Tytler (1998a); 8: Pettini & Bowen (2001).

^bRelative to the solar value $\log(\text{O/H})_{\odot} + 12 = 8.66$ (Asplund, Grevesse & Sauval 2005).

^cThis is a very conservative upper limit on the metallicity. Burles & Tytler (1998b) estimate $[\text{Si/H}] \simeq -2.5$ and $[\text{C/H}] \simeq -2.9$ from photoionisation modelling.

the individual measure of $\log(\text{D/H})$ in Table 3 to obtain the weighted mean $\langle \log(\text{D/H})_{\text{p}} \rangle = -4.55 \pm 0.02$. However, the scatter of the points about this value is rather high for the quoted error bars assuming a Gaussian error model, giving $\chi^2 = 19$ which formally corresponds to a high probability that a further independent experiment would obtain a better fit to the data, $P(\chi^2 > 19) < 0.01$. This suggests that the errors on the individual measures of D/H may have been underestimated – a well known and much discussed (e.g. Steigman 2007) ‘problem’ of the determination of $(\text{D/H})_{\text{p}}$ from QSO spectra. An alternative, and more conservative, method of estimating the error on the weighted mean would attempt to account for the actual scatter in the data. One possibility is to consider the mean and standard deviation of a large number of weighted means generated by random sampling (with substitution) of the seven observed values (the bootstrap method; see Efron & Tibshirani 1993). In this way we obtain:

$$\langle \log(\text{D/H})_{\text{p}} \rangle = -4.55 \pm 0.03$$

A more Bayesian approach could try to account for uncertainty in the error bars using the observed scatter in the data. For example, fitting a Gaussian model with the variance on each point increased by a constant to $\sigma_i^2 + \delta\sigma^2$ shows that the data prefer values of $\delta\sigma > 0$. Using the maximum likelihood value $\delta\sigma \sim 0.07$ gives a posterior constraint on $\langle \log(\text{D/H})_{\text{p}} \rangle$ consistent with the bootstrap estimate above, as does marginalizing over $\delta\sigma^2$ with prior $\propto 1/(0.02^2 + \delta\sigma^2)$ (though the distribution is somewhat non-Gaussian). Using a model that multiplicatively increases the noise gives similar results.

The scatter in the reported determinations of D/H in QSO absorbers is illustrated in Figure 4. Out of the seven measurements, there are two which lie outside the confidence intervals of the mean by more than 1σ : Q1009+299 and Q2206-199. If we consider these two cases more closely we can find, in retrospect, plausible reasons why their 1σ errors may have been underestimated. The partial Lyman limit system in line to Q1009+299 has the lowest column density among the sample, $\log[N(\text{H I})/\text{cm}^{-2}] = 17.39$, and is unique among the ones considered here in showing D I absorption in only *one* line, Ly α , the column density of D I being too low

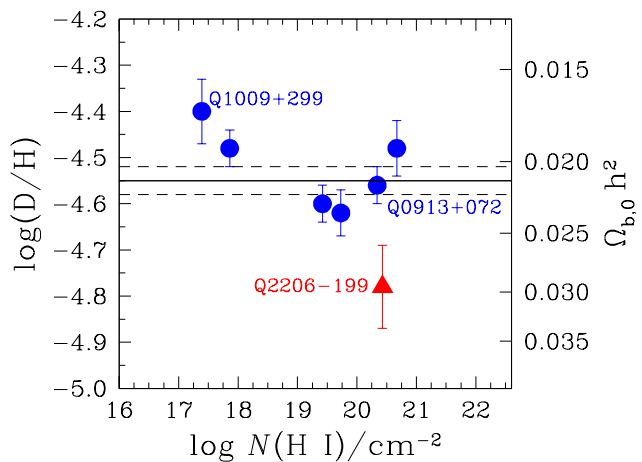


Figure 4. Measures of deuterium abundance in high redshift QSO absorbers. Only cases where the deuterium absorption is clearly resolved from nearby spectral features are shown here (see text). Blue circles denote systems observed from the ground with 8-10 m telescopes and echelle spectrographs, while the red triangle refers to lower resolution observations made with the *Hubble Space Telescope*. Absorption systems discussed in the text are labelled with the name of the background QSO. The horizontal lines are drawn at the weighted mean value of $\log(\text{D/H})$ and its error, as determined with the bootstrap method.

to produce discernible absorption in higher order lines. The $z_{\text{abs}} = 2.07624$ DLA towards Q2206-199 is the lowest redshift absorber in the sample, requiring space-borne observations to record the high order lines where D I absorption can be resolved from H I. The *HST*-STIS spectrum of this object published by Pettini & Bowen (2001) is of lower S/N ratio and resolution than the other six cases in Table 3 which were all obtained with ground-based 8-10 m telescopes and echelle spectrographs. If we arbitrarily double the 1σ estimates of the errors in the determinations of D/H in Q1009+299 and Q2206-199 reported in the original works, we find the same weighted mean $\langle \log(\text{D/H})_{\text{p}} \rangle = -4.55 \pm 0.02$ as before, but a much reduced $\chi^2 = 11$ ($P(\chi^2 > 11) \simeq 0.1$).

In conclusion, the value of D/H we deduce here for the $z_{\text{abs}} = 2.61843$ DLA in the spectrum of Q0913+072 is in good agreement with four out of the previous six determinations generally considered to be the most reliable. Its inclusion in the ‘prime’ sample, helps identify two outliers and plausible reasons for much of the scatter among the sample. The weighted mean $\langle \log(D/H)_p \rangle$ is unchanged compared to the most recent previous estimate of this quantity by O’Meara et al. (2006), leading us to conclude that the true value of the primordial abundance of deuterium lies in the range:

$$\langle \log(D/H)_p \rangle = -4.55 \pm 0.03 \quad (6)$$

at the 68% confidence level.

4.1 The cosmological density of baryons from $(D/H)_p$

Steigman (2007) has pointed out that in the range of interest here the primordial abundance of D is simply related via the expression

$$10^5(D/H)_p = 2.67(1 \pm 0.03) (6/\eta_{10})^{1.6} \quad (7)$$

to η_{10} which measures the universal ratio of the densities of baryons and photons in units of 10^{-10} :

$$\eta_{10} \equiv 10^{10}(n_b/n_\gamma) = 273.9\Omega_{b,0}h^2 \quad (8)$$

The 3% uncertainty in eq. (7) is comparable to the uncertainties in the nuclear reaction rates used in Big-Bang nucleosynthesis codes. The conversion from η_{10} to $\Omega_{b,0}h^2$ in eq. (8) is accurate to about 0.1% (Steigman 2006). From eqs. (6), (7) and (8), we find:

$$\Omega_{b,0}h^2(\text{BBN}) = 0.0213 \pm 0.0009 \pm 0.0004 \quad (9)$$

where the error terms reflect the uncertainties in, respectively, $(D/H)_p$ (eq. 6) and the nuclear reaction rates (eq. 7). Combining the two error terms in quadrature, we have:

$$\Omega_{b,0}h^2(\text{BBN}) = 0.0213 \pm 0.0010 \quad (10)$$

The analysis by Dunkley et al. (2008) of five years of observations with the *WMAP* satellite concluded that, on the basis of the *WMAP* data alone

$$\Omega_{b,0}h^2(\text{CMB}) = 0.02273 \pm 0.00062. \quad (11)$$

The two estimates of $\Omega_{b,0}h^2$ agree (just) within the errors; we also note that the uncertainty from BBN is now comparable to that from the CMB. Given that the best-fitting value of $\Omega_{b,0}h^2(\text{CMB})$ is tied to those of other cosmological parameters, it is of interest to consider the effect of including the value of $\Omega_{b,0}h^2(\text{BBN})$ as a prior in the analysis of the *WMAP* 5 data.

5 COMBINED CONSTRAINTS ON COSMOLOGICAL PARAMETERS FROM THE CMB AND $(D/H)_p$

The five-year *WMAP* CMB temperature maps and large scale polarization maps together provide tight constraints on several combinations of cosmological parameters (Hinshaw et al. 2008; Dunkley et al 2008). In order to constrain *individual* parameters, however, it helps to apply external

data that can break degeneracies. The baryon density, which affects the relative heights of the CMB acoustic peaks, is partly degenerate with the spectral index of primordial fluctuations, n_s , since *WMAP* provides precision measurements of only two peaks in the temperature power spectrum. Increasing the value of n_s increases the height of the second peak, which can be compensated by a decrease in the baryon density. Hence we can get a better constraint on the spectral index by combining the CMB data with an independent determination of $\Omega_{b,0}h^2$.

Among the alternative avenues to $\Omega_{b,0}$ which have been considered, the primordial abundance of deuterium is the most accurate at present. The baryonic acoustic oscillations imprinted in the large-scale distribution of galaxies currently provide less stringent constraints on $\Omega_{b,0}$ than either the CMB or $(D/H)_p$ and, in any case, really measure the combination of parameters $\Omega_{b,0}/\Omega_{m,0}h$ (e.g. Blake et al. 2007). Measurements of other light elements created in Big-Bang nucleosynthesis suffer from systematic uncertainties which are difficult to quantify (in the case of helium) or are poorly understood (for lithium), as discussed in recent reviews by Molaro (2008) and Steigman (2007) (see also Simha & Steigman 2008). In considering only deuterium in our joint analysis with the CMB we make the implicit assumption that at present the primordial abundances of ${}^4\text{He}$ and ${}^7\text{Li}$ are difficult to reconcile with that of D because of astrophysical considerations (such as how to extrapolate from measured values in local astrophysical environments to the primordial abundances) and do not reflect an underlying departure from standard Big-Bang nucleosynthesis. If the latter were the case, we would be unjustified in comparing the CMB fluctuations with only $(D/H)_p$.

Parameter constraints from CMB data are usually encoded in a set of samples from the posterior distribution generated from the likelihood function by Markov Chain Monte Carlo methods. In combining the CMB data with the value reached here from $(D/H)_p$, $\Omega_{b,0}h^2(\text{BBN}) = 0.0213 \pm 0.0010$, we assume that the baryon density likelihood is an uncorrelated Gaussian. Since the constraint is only on one parameter, and consistent with the baryon density inferred from the CMB alone, we can use importance sampling to re-weight the parameter samples with the extra constraint (see Lewis & Bridle 2002 for details). For each sample in the original chain supplied by the *WMAP* team,⁴ we weight the sample by $\exp[-(\Omega_{b,0}h^2 - 0.0213)^2/(2 \times 0.001^2)]$. Marginalized constraints for individual parameters can be calculated easily from the weighted chains; we use the ‘GetDist’ program provided with CosmoMC (Lewis & Bridle 2002) to do this.

5.1 Standard Λ CDM cosmological model

We assume the simplest flat Λ CDM cosmological model, with a power-law purely adiabatic spectrum of linear primordial curvature perturbations with spectral index n_s and amplitude A_s at $k = 0.002 \text{ Mpc}^{-1}$, dark matter density $\Omega_{c,0}h^2$, baryon density $\Omega_{b,0}h^2$, optical depth for sharp reionization τ , and cosmological constant density relative to critical $\Omega_{\Lambda,0}$

⁴ Available from:

<http://lambda.gsfc.nasa.gov/product/map/dr3/parameters.cfm>

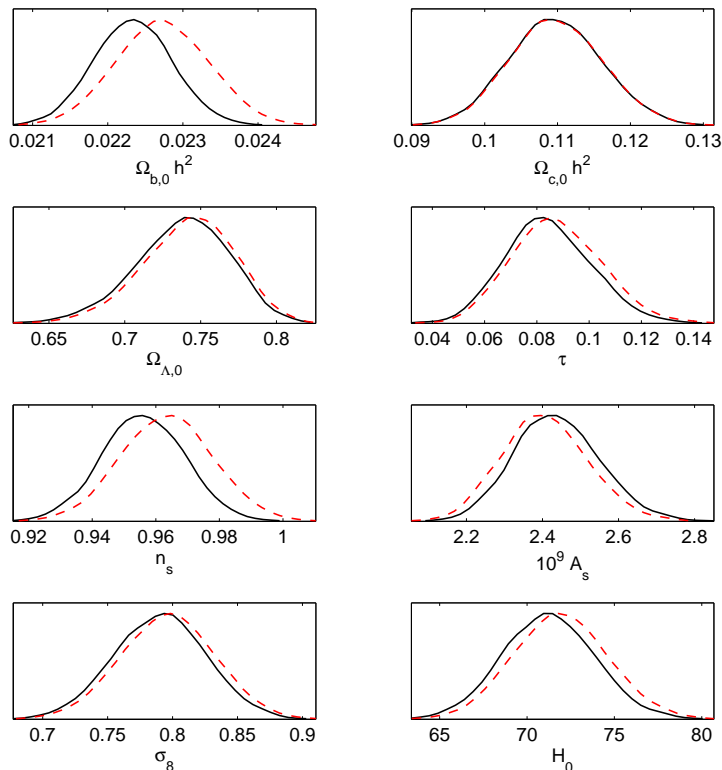


Figure 5. Probability distributions of cosmological parameters deduced from the analysis of *WMAP 5* data alone (red dashed line) and including $\Omega_{b,0}h^2(\text{BBN})$ as a prior (black continuous line).

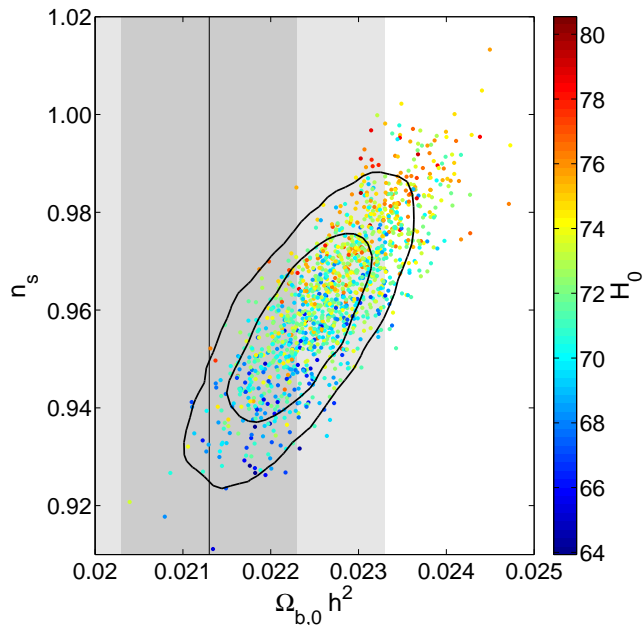


Figure 6. The points show pairs of values of the baryon density, $\Omega_{b,0}h^2$, and the spectral index of primordial fluctuations, n_s , implied by the *WMAP* data alone, colour-coded according to their value of the Hubble parameter H_0 (in units of $\text{km s}^{-1} \text{Mpc}^{-1}$). The vertical line shows the value of $\Omega_{b,0}h^2(\text{BBN})$, with the shaded regions showing the 1σ and 2σ bounds from eq. (10). The contours are the 1σ and 2σ constraints obtained by combining the *WMAP* data with $(\text{D}/\text{H})_p$.

(with a flat prior). Marginalized one-dimensional parameter constraints obtained in this way are shown in Fig. 5.

The combined constraint on the baryon density is $\Omega_{b,0}h^2 = 0.0223 \pm 0.0005$ where the error corresponds to the 68% probability from the distribution shown in the top left-hand panel of Fig. 5. For comparison, the value obtained by combining the *WMAP 5* data with the distance measurements from Type Ia supernovae and the baryon acoustic oscillations in the large-scale distribution of galaxies is $\Omega_{b,0}h^2 = 0.02265 \pm 0.0006$ (Komatsu et al. 2008).

Since the $(\text{D}/\text{H})_p$ measurement prefers values of the baryon density towards the lower end of the range allowed by the CMB, inclusion of this prior leads to a lower value of the spectral index: we obtain $n_s = 0.956 \pm 0.013$, and $n_s < 0.990$ at 99% confidence (purely statistical errors). Thus, red spectral tilts are preferred and a Harrison-Zeldovich spectrum with $n_s = 1$ is ruled out in the simplest ΛCDM models. Other parameter constraints are almost unchanged, with only slight shifts in τ , σ_8 and H_0 towards lower values. The combined goodness-of-fit parameter χ_{eff}^2 increases by about one on including the $\Omega_{b,0}h^2(\text{BBN})$ constraint, consistent with expectations for adding one independent parameter. Figure 6 shows the combined constraints on n_s and $\Omega_{b,0}h^2$ with and without inclusion of the $(\text{D}/\text{H})_p$ prior.

5.2 Constraints on a tensor component to primordial fluctuations

If the spectral index is less than one, some inflationary models predict an observable amplitude of primordial gravitational waves. Adding a parameter r (with flat prior)

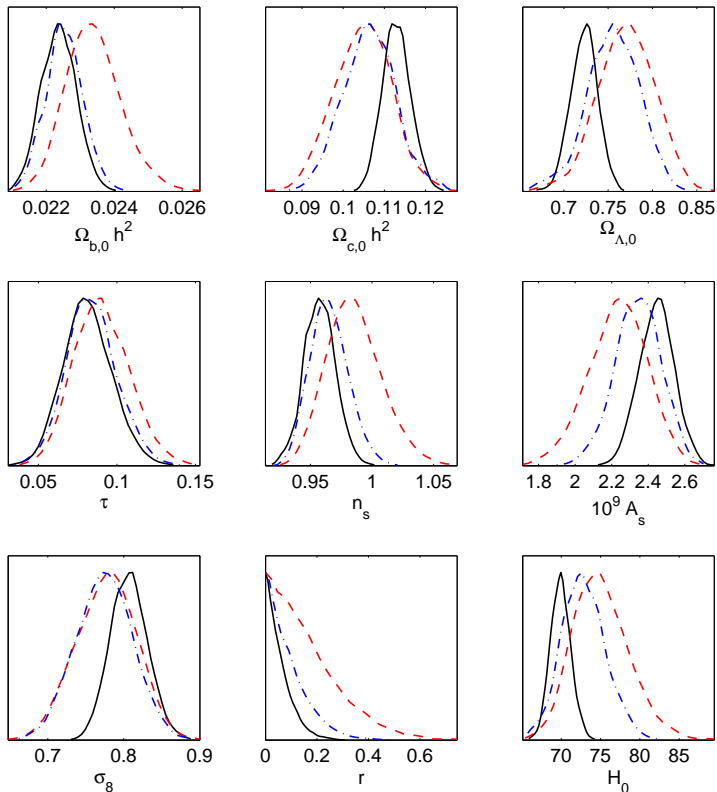


Figure 7. Probability distributions of cosmological parameters deduced from the analysis of: (i) *WMAP 5* data alone (red dashed line); (ii) *WMAP 5* + $(D/H)_p$ (blue dot-dash line); (iii) adding to (ii) the constraints imposed by baryon acoustic oscillations in the large-scale distribution of galaxies and by the distances to Type Ia supernovae (black continuous line – see text for relevant references).

to measure the ratio of the tensor and scalar power at $k = 0.002 \text{ Mpc}^{-1}$, is therefore well motivated (using the relation between the tensor and scalar tilts for the simplest inflation models; see Komatsu et al. 2008). A combination of *WMAP 5* data and the $(D/H)_p$ constraint then gives $n_s < 1.00$, and a limit on the tensor amplitude $r < 0.26$, both at 95% confidence. The constraints on these parameters are consistent with, and comparable to, those obtained by Komatsu et al. (2008) by considering *WMAP* data in conjunction with baryon oscillations and supernova distances measurements, but have completely different systematics. Considering all the constraints together – *WMAP 5*, $(D/H)_p$, Type Ia supernovae (Riess et al. 2004; Astier et al. 2006; Wood-Vasey et al. 2007), and baryon acoustic oscillations in the large-scale distribution of galaxies (Percival et al. 2007) – we arrive at the full joint probability distributions shown by the black continuous lines in Fig. 7. We find $r < 0.16$ at 95% confidence and $n_s < 0.994$ at 99% confidence. These limits strongly constrain possible models of the early universe, but are consistent with some of the simplest inflationary (and other) models. Joint marginalized constraints on the various parameters are: $\Omega_{b,0}h^2 = 0.0224 \pm 0.0005$, $\Omega_{c,0}h^2 = 0.1130 \pm 0.0034$, $\Omega_{\Lambda,0} = 0.723 \pm 0.015$, $h = 0.700 \pm 0.013$, $n_s = 0.959 \pm 0.013$, $\sigma_8 = 0.808 \pm 0.025$, and $\tau = 0.818 \pm 0.016$ (1σ errors).

5.3 A closer look at the impact of the errors on D/H on the derivation of cosmological parameters

The results presented in Sections 5.1 and 5.2 assumed a Gaussian error on $\Omega_{b,0}h^2$ (BBN) derived from the dispersion of D/H measurements analysed with the bootstrap method. However, values for high-significance confidence limits are quite sensitive to the shape of the tails of the distribution and it is therefore worth assessing the robustness of our results to changes in the statistical model.

As discussed in Section 4, a Bayesian model that increases the error bars by some constant and marginalizes over the possible values of the constant gives an error estimate on $\langle (D/H)_p \rangle$ which is comparable to that obtained with the bootstrap method. However, the tails of the distributions have quite different shapes. Fig. 8 shows the result of numerically evaluating the distribution of $\Omega_{b,0}h^2$, assuming Gaussian errors on the $\log(D/H)$ measurements, marginalizing over the additional error variance with a Jeffrey-like (i.e. inverse) prior on its amplitude, and including the 3% error (also assumed to be Gaussian) in the relation between η_{10} and $(D/H)_p$ (eq. 7). The broad tails arise from marginalization over relatively large values of the added error variance, and fall off as a power law, rather than exponentially as in the bootstrap model. The result is not very sensitive to the inclusion or exclusion of the two most outlying data points in Fig. 4.

Using the marginalized results for additive additional

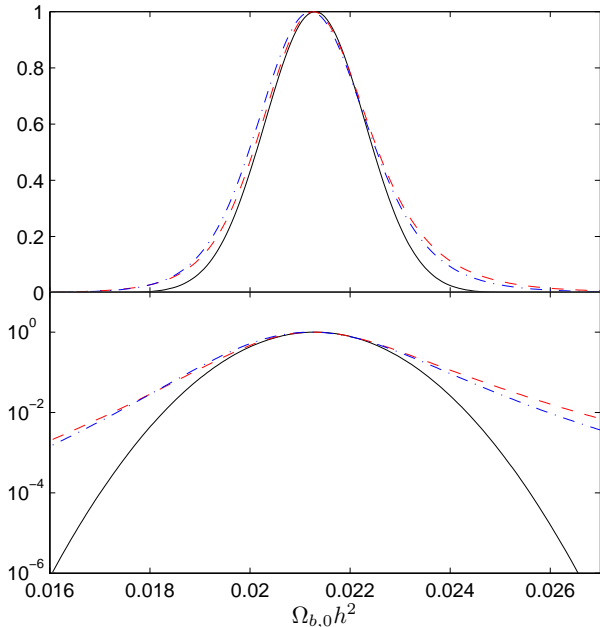


Figure 8. Likelihood distributions for $\Omega_{b,0}h^2$ (BBN) for different statistical models of the errors in the seven D/H measurements considered here (see Table 3). The solid line is a Gaussian with $\Omega_{b,0}h^2 = 0.0213 \pm 0.0010$ (eq. 10). The other curves show the result of marginalizing over an increased error variance adding to (red dashed) or multiplying (blue dot-dashed) the errors on the individual D/H determinations reported in the original works. The additional error variance has a Jeffrey-like (regularized inverse amplitude) prior. All errors are assumed to be uncorrelated, and the results are normalized to peak at 1.

error variance, the parameter constraints change somewhat from the values given in sections 5.1 and 5.2. For example, combining the numerical baryon density likelihood with *WMAP 5* data for tensor models, the 95% limit on n_s changes from $n_s < 1.00$ to $n_s < 1.01$ due to the tail of higher $\Omega_{b,0}h^2$ values that are now allowed. The combined tightest constraints change to $\Omega_{b,0}h^2 = 0.0226 \pm 0.0006$, $n_s = 0.961 \pm 0.014$, with $n_s \geq 1$ still just excluded at 99% confidence and $r < 0.17$ at 95% confidence.

In both the Bayesian and bootstrap model, our results depend critically on the assumption that the quoted errors on the individual determinations of (D/H) in Table 3 (original and inflated) are statistically independent and Gaussian. The changes in the values of (or limits on) $\Omega_{b,0}h^2$, n_s , and r which we have just noted when changing the statistical model of the errors give an indication of the systematic error in the result due to the likelihood model, even when these assumptions are satisfied. In future, with a larger sample of measurements of (D/H) in QSO absorbers, it may be possible to test the assumptions that the errors are independent and Gaussian, and perhaps identify the origin of the excess scatter in the existing measurements. Such improvements would allow the primordial abundance of deuterium to fulfil its potential in constraining cosmological parameters. On a different note, the Planck satellite should independently measure the baryon density from the CMB alone with $\sim 0.6\%$ accuracy in a few years, with measurements of several acoustic peaks breaking the degeneracy with n_s .

6 SUMMARY AND CONCLUSIONS

The lowest metallicity damped Ly α systems are good candidates for the measurement of the primordial abundance of deuterium, not only because the gas has suffered little astration, but also because they preferentially arise in gas clouds with low internal velocity dispersions, facilitating the resolution of the isotope shift of 82 km s^{-1} . Furthermore, the high column densities involved give detectable D I absorption in many lines of the Lyman series. The $z_{\text{abs}} = 2.61843$ DLA in the spectrum of the bright QSO Q0913+072 is a good case in point – we have reported here high S/N ratio detections of six D I absorption lines from which we deduce $\log(D/H) = -4.56 \pm 0.04$. The main contribution to the error in $\log(D/H)$ is from the uncertainty in the column density of H I, rather than D I; it may be possible to reduce this further in future with more sophisticated modelling of the Lyman forest absorption that is superimposed on the wide, damped profile of the Ly α line.

The value of D/H we deduce for this DLA is in good agreement with those of four out of the six QSO absorbers previously considered to constitute the most reliable set of such determinations. The other two differ from the mean of the whole sample by $\sim 2\sigma$, and we have identified possible reasons why their errors may have been underestimated in the original reports. We propose that the determination of the primordial abundance of deuterium is converging towards the value $\langle \log(D/H)_p \rangle = -4.55 \pm 0.03$, which can be considered reliable within the 68% confidence limits. The corresponding $\Omega_{b,0}h^2$ (BBN) = 0.0213 ± 0.0010 agrees within the errors with $\Omega_{b,0}h^2$ (CMB) = 0.02273 ± 0.00062 . Including the former as a prior in the analysis of the *WMAP 5* data from which the latter is deduced results in a lower mean value of the power-law index of primordial fluctuations, from $n_s = 0.963 \pm 0.015$ to $n_s = 0.956 \pm 0.013$. The effects on other cosmological parameters deduced from the analysis of the CMB are more modest. Considering together the constraints available from *WMAP 5*, (D/H)_p, baryon oscillations in the galaxy distribution, and distances to Type Ia supernovae, we arrive at the current best estimates $\Omega_{b,0}h^2 = 0.0224 \pm 0.0005$, $n_s = 0.959 \pm 0.013$ (1σ errors), and $r < 0.16$ (2σ limit) for the ratio of the tensor and scalar power at $k = 0.002 \text{ Mpc}^{-1}$.

Despite the long integration time, the data presented here have not led to a significant change in the estimate of (D/H)_p compared with the last paper to report new observations (O’Meara et al. 2006). This is a good sign; together with the agreement between $\Omega_{b,0}h^2$ (BBN) and $\Omega_{b,0}h^2$ (CMB), it suggests that we have reached a stage where the primordial abundance of deuterium and the cosmological density of baryons are sufficiently well determined quantities. There is now less urgency to increase further the number of D/H measurements in QSO absorbers, although a ‘prime’ sample of only seven data points clearly does not allow for complacency. In particular, an expanded sample of D/H measures at high redshifts would improve the statistical model on which the errors on the derived cosmological parameters are based. The most metal-poor DLAs remain a fertile ground for studying early episodes of *stellar* nucleosynthesis (e.g. Pettini et al. 2008), and it is certainly worthwhile continuing to be aware of their potential for further refinements of (D/H)_p.

ACKNOWLEDGMENTS

The work presented in this paper is based on UVES observations made with the European Southern Observatory VLT/Kueyen telescope at Paranal, Chile, obtained in programme 078.A-0185(A) and from the public data archive. We are grateful to the ESO time assignment committee, and to the staff astronomers at VLT for their help in conducting the observations. Bob Carswell, Jim Lewis, and Sam Rix kindly helped with various aspects of the data analysis, and John O'Meara and Gary Steigman offered valuable comments on an earlier version of the paper. We also thank the anonymous referee for useful suggestions on the presentation of the data. We acknowledge the use of the Legacy Archive for Microwave Background Data Analysis (LAMBDA). Support for LAMBDA is provided by the NASA Office of Space Science. MTM thanks the Australian Research Council for a QEII research fellowship (DP0877998). CCS's research is partly supported by grant AST-0606912 from the US National Science Foundation.

REFERENCES

- Adams, T. F. 1976, *A&A*, 50, 461
- Akerman, C. J., Ellison, S. L., Pettini, M., & Steidel, C. C. 2005, *A&A*, 440, 499
- Asplund, M., Grevesse, N., & Sauval, A. J. 2005, in Barnes T. G., III, Bash F. N., eds, *ASP Conf. Ser. Vol. 336, Cosmic Abundances as Records of Stellar Evolution and Nucleosynthesis*, Astron. Soc. Pac., San Francisco, p. 25
- Astier, P., et al. 2006, *A&A*, 447, 31
- Blake, C., Collister, A., Bridle, S., & Lahav, O. 2007, *MNRAS*, 374, 1527
- Bridle, S. L., Lahav, O., Ostriker, J. P., & Steinhardt, P. J. 2003, *Science*, 299, 1532
- Burles, S., Tytler, D. 1998a, *ApJ*, 499, 699
- Burles, S., Tytler, D. 1998b, *ApJ*, 507, 732
- Crighton, N. H. M., Webb, J. K., Ortiz-Gil, A., & Fernández-Soto, A. 2004, *MNRAS*, 355, 1042
- Dekker, H., D'Odorico, S., Kaufer, A., Delabre, B., & Kotzlowski, H. 2000, in Masanori, I., Moorwood, A. F. M., eds., *Proc SPIE, Vol. 4008, Optical and IR Telescope Instrumentation and Detectors*. SPIE, Bellingham, p. 534
- Dunkley, J. et al. 2008, *ApJS*, submitted (arXiv:0803.0586)
- Efron, B., Tibshirani, R. J. 1993, *An Introduction to the Bootstrap*. Chapman & Hall, New York
- Erni, P., Richter, P., Ledoux, C., & Petitjean, P. 2006, *A&A*, 451, 19
- Hinshaw, G., et al. 2008, *ApJS*, submitted (arXiv:0803.0732)
- Hobbs, L. M. 1974, *ApJ*, 191, 381
- Kirkman, D., Tytler, D., Suzuki, N., O'Meara, J. M., Lubin, D. 2003, *ApJS*, 149, 1
- Komatsu, E., et al. 2008, *ApJS*, submitted (arXiv:0803.0547).
- Ledoux, C., Petitjean, P., Bergeron, J., Wampler, E. J., Srianand, R. 1998, *A&A*, 337, 51
- Ledoux, C., Petitjean, P., Fynbo, J. P. U., Møller, P., & Srianand, R. 2006, *A&A*, 457, 71
- Levshakov, S. A., Dessauges-Zavadsky, M., D'Odorico, S., & Molaro, P. 2002, *ApJ*, 565, 696
- Lewis, A., & Bridle, S. 2002, *Phys. Rev. D*, 66, 103511
- Linsky, J. L., et al. 2006, *ApJ*, 647, 1106
- Molaro, P. 2008, in Knapen, J. H., Mahoney, T. J., Vazdekis, A. eds, *ASP Conf. Ser. Vol. 390, Pathways Through an Eclectic Universe*. Astron. Soc. Pac., San Francisco, p. 472
- Morton, D. C. 2003, *ApJS*, 149, 205
- Murphy, M. T., Curran, S. J., Webb, J. K., Ménager, H., & Zych, B. J. 2007, *MNRAS*, 376, 673
- O'Meara, J. M., Burles, S., Prochaska, J. X., Prochter, G. E. 2006, *ApJ*, 649, L61
- O'Meara, J. M., Tytler, D., Kirkman, D., Suzuki, N., Prochaska, J. X., Lubin, D., Wolfe, A. M. 2001, *ApJ*, 552, 718
- Percival, W. J., Cole, S., Eisenstein, D. J., Nichol, R. C., Peacock, J. A., Pope, A. C., & Szalay, A. S. 2007, *MNRAS*, 381, 1053
- Pettini, M. 2006, in Sonneborn, G., Moos, W., Andersson, B.-G., eds, *ASP Conf. Ser. Vol. 348, Astrophysics in the Far Ultraviolet: Five Years of Discovery with FUSE*. Astron. Soc. Pac., San Francisco, p. 19
- Pettini, M., Bowen, D. V. 2001, *ApJ*, 560, 41
- Pettini, M., Smith, L. J., King, D. L., Hunstead, R. W. 1997, *ApJ*, 486, 665
- Pettini, M., Zych, B. J., Steidel, C. C., Chaffee, F. H. 2008, *MNRAS*, 385, 2011
- Pontzen, A., Governato, F., Pettini, M., Booth, C. M., Stinson, G., Wadsley, J., Brooks, A., Quinn, T., Haehnelt, M. 2008, *MNRAS*, in press (arXiv:0804.4474)
- Prantzos, N., & Ishimaru, Y. 2001, *A&A*, 376, 751
- Prochaska, J. X., Chen, H.-W., Wolfe, A. M., Dessauges-Zavadsky, M., Bloom, J. S. 2008, *ApJ*, 672, 59
- Riess, A. G., et al. 2004, *ApJ*, 607, 665
- Romano, D., Tosi, M., Chiappini, C., & Matteucci, F. 2006, *MNRAS*, 369, 295
- Savage, B. D., & Sembach, K. R. 1991, *ApJ*, 379, 245
- Simha, V., & Steigman, G. 2008, *Journal of Cosmology and Astro-Particle Physics*, 6, 16
- Steigman, G. 2006, *Journal of Cosmology and Astro-Particle Physics*, 10, 16
- Steigman, G. 2007, *ARNPS*, 57, 463
- Steigman, G., Romano, D., Tosi, M. 2007, *MNRAS*, 378, 576
- Strömgren, B. 1948, *ApJ*, 108, 242
- Tytler, D., Fan, X.-M., Burles, S., Cottrell, L., Davis, C., Kirkman, D., Zuo, L. 1995, in Meylan, G., ed, *QSO Absorption Lines*. Springer-Verlag, Berlin, p. 289
- Wolfe, A. M., Gawiser, E., & Prochaska, J. X. 2005, *ARA&A*, 43, 861
- Wood-Vasey, W. M., et al. 2007, *ApJ*, 666, 694

APPENDIX A: UVES SPECTRUM OF Q0913+072

For the interested reader, we provide the final reduced and co-added UVES spectrum of Q0913+072, as used in the work reported here and in Pettini et al. (2008). Relevant details are given in Section 2. The spectrum is available in its entirety in the electronic edition of the journal. A portion is shown here for guidance regarding its form and content.

Wavelength ^a (Å)	Relative Flux (Arbitrary Units)	1 σ Error in Relative Flux
3.2999990E+03	-4.8096318E+00	1.9800955E+01
3.3000266E+03	7.2700119E+01	2.1541672E+01
3.3000540E+03	8.8452042E+01	1.9596445E+01
3.3000815E+03	6.0643616E+01	1.8316561E+01
3.3001091E+03	5.9261909E+01	2.0739399E+01
3.3001367E+03	-8.5954037E+00	2.0203918E+01
3.3001641E+03	6.8833572E-01	1.9290850E+01
3.3001917E+03	9.1782742E+00	1.8983492E+01
3.3002192E+03	-8.3213625E+00	2.0355886E+01
3.3002468E+03	2.1003305E+01	2.0274757E+01

^aVacuum heliocentric.